

The nonstoichiometry and physical properties of the $\text{Nd}_{1-x}\text{Ca}_{1+x}\text{FeO}_{4-y}$ system

SUNG GYUN ROH, KWON SUN ROH, CHUL HYUN YO
Department of Chemistry, Yonsei University, Seoul, 120-749, Korea

The solid solutions of the $\text{Nd}_{1-x}\text{Ca}_{1+x}\text{FeO}_{4-y}$ system for compositions of $x=0.000, 0.125, 0.250, 0.375,$ and 0.500 are prepared by drip pyrolysis. XRD analysis shows all the solid solutions are tetragonal $I_{4/mmm}$. The Fe^{4+} ratio to the total Fe ions or τ value has a maximum for the composition $x=0.375$. From the X-ray powder diffraction analysis and the Mössbauer spectroscopy, the distortion and symmetry change of oxygen octahedra of Fe ions are observed. The structural change of oxygen octahedra of Fe ions strongly affects the physical properties. The solid solution when $x=0.000$ shows a weak ferromagnetic behaviour due to the spin canting of the distorted octahedra. The other solid solutions with $x=0.125, 0.250, 0.375,$ and 0.500 show a paramagnetic behaviour over room temperature. The decrease of the magnetic transition temperature is due to the distortion of oxygen octahedra of Fe ions and the existence of the Fe^{4+} ion. The formation site of oxygen vacancies plays an important role in the conductivity of the $\text{Nd}_{1-x}\text{Ca}_{1+x}\text{FeO}_{4-y}$ system. Although the oxygen vacancies in [Nd, Ca]–O layer have little effect on conductivity, the oxygen vacancies in the FeO_2 plane of the perovskite layer act as electron trapping sites and thus increase the activation energy.

1. Introduction

ABO_3 perovskite [1] and K_2NiF_4 -type structures [2] corresponding to $n = \infty$ and $n = 1$, respectively, in the Ruddlesden–Popper type compound series of $\text{AO}(\text{ABO}_3)_n$ or $\text{A}_{n+1}\text{B}_n\text{O}_{3n+1}$, have shown interesting and special physical properties and therefore they have been studied extensively. Whereas ABO_3 perovskites form three-dimensional octahedra networks, the ideal tetragonal K_2NiF_4 structures are composed of alternating perovskite (ABO_3) and rock salt (AO) layers along the tetragonal c -axis. Thus the K_2NiF_4 compounds exhibit two-dimensional magnetic and electrical properties through ab -plane B–O–B bonds of two-dimensional corner sharing octahedra networks in the perovskite layer. More precisely, an ABO_3 perovskite layer is composed of AO and BO_2 layers and the sequence along the c -axis in the K_2NiF_4 structure is BO_2 –AO–AO– BO_2 –AO–AO– BO_2 in which oxygen atoms at the apices of the BO_6 octahedron are simultaneously a part of the AO layer.

Physical properties of the K_2NiF_4 -type compounds are greatly affected by the mixed valencies of B-site ions and oxygen vacancies because magnetic and electrical interactions are determined by the ab -plane B–O–B bonds in the perovskite layer. However, the oxygen vacancies in the BO_2 and AO layers in the K_2NiF_4 structure have different influences on physical properties. In general, the K_2NiF_4 -type compounds show thermally activated electrical conductivity and the antiferromagnetic interaction exhibited by the superexchange model.

Although interplanar couplings between B site ions in the perovskite layers of CaLaFeO_4 magnetic structure are antiferromagnetic, the magnetic moments are aligned in the (001) plane along the a -axis and magnetic ordering appears at 373 K [3]. Different magnetic arrangements in LaSrFeO_4 compound may be considered as intraplanar antiferromagnetic interactions and then a magnetic ordering appears at 380 K [4]. The stability of the K_2NiF_4 compounds can be estimated by the Goldschmidt tolerance factor ($0.85 \leq t \leq 1.02$) [5]. If the t value is less than unity, a bond mismatch occurs between the rock salt and the perovskite layer, which introduces a tensile stress in the rock salt (AO) layer and a compression stress in the perovskite (ABO_3) layer [2]. Thus the B–O bonds of the K_2NiF_4 -type compound are smaller than those of perovskite. If t approaches low or high limits, it can not be accommodated by B–O bond shrinkage and then structural changes occur [6]. The structure and physical properties of the K_2NiF_4 compounds are greatly influenced by the t value. The K_2NiF_4 compounds also can adopt considerable oxygen vacancies and recent study shows that there are different oxygen vacancy arrangements between the $\text{Ca}_2\text{FeO}_{3.5}$ and $\text{Ca}_2\text{MnO}_{3.5}$ compounds [7].

In the present study, the solid solutions of the $\text{Nd}_{1-x}\text{Ca}_{1+x}\text{FeO}_{4-y}$ system ($x = 0.000, 0.125, 0.250, 0.375,$ and 0.500) have been prepared and analysed by the X-ray powder diffraction method, Mohr salt titration, and Mössbauer spectroscopy. The nonstoichiometric chemical formulas of the solid solutions could be formulated by the Mohr analysis. Observed

magnetic and electrical properties are discussed with relation to the mixed valence state of Fe ions, oxygen vacancy, two-dimensional structure, and the degree of Fe–O covalency.

2. Experimental procedure

The solid solutions of the $\text{Nd}_{1-x}\text{Ca}_{1+x}\text{FeO}_{4-y}$ system ($x = 0.000, 0.125, 0.250, 0.375,$ and 0.500) were prepared by drip pyrolysis and heat-treatment at 1350°C under atmospheric air pressure. The starting materials such as Nd_2O_3 (99.99%), CaCO_3 (99.99%), and $\text{Fe}(\text{NO}_3)_3 \cdot 9\text{H}_2\text{O}$ (analytical grade) were weighed in appropriate stoichiometric amounts and dissolved in dilute nitric acid and then the solution dripped onto the hot surface of a long quartz tube at 800°C in an electrical furnace. The solution when dropped onto the hot quartz surface produced localized ignition sites which gave a very fine ash of intermediate state phases which were subsequently heated at 1350°C at ambient atmosphere for 48 h and then annealed at 850°C for 24 h. The regrinding and heating processes were repeated several times in order to obtain a single phase product.

The phase of the solid solution was identified by X-ray powder analysis with a Philips pw 1710 diffractometer using monochromatized CuK_α ($\lambda = 0.15418$ nm) radiation. Lattice parameters, lattice volume of the unit cell, and crystal system of the solid solutions were determined accordingly.

The oxidation states of iron ions were determined by the Mohr salt analysis in which a given amount of sample was dissolved in 0.1 N solution of Mohr salt with small amounts of HCl and titrated with 0.1 N $\text{K}_2\text{Cr}_2\text{O}_7$ standard solution. The mole ratio of the Fe^{4+} to total iron ions, oxygen vacancy and non-stoichiometric chemical formulas for the system were determined from the analysis.

The Mössbauer spectra were recorded at room temperature using 14.4 keV ^{57}Co γ -ray radiation and fitted to the Lorentzian curve using PC-MOS to obtain Mössbauer parameters such as isomer shift, quadrupole splitting, and magnetic hyperfine field.

The electrical conductivity measurements of the polycrystalline pellet samples have been carried out by the four-probe d.c. technique in the temperature range 278 to 900 K for the composition with $x = 0.000$ and in the range 145 to 278 K for the compositions with $x = 0.125, 0.250, 0.375,$ and 0.500 . The electrical conductivities were calculated using Laplume's equation and the activation energy is estimated from the slope on the Arrhenius plot of the conductivity.

The magnetic susceptibilities were measured using a Faraday balance from room temperature to 800 K. The solid solution with $x = 0.000$ shows magnetic field dependence and therefore was measured under two different magnetic fields.

3. Results and discussion

The solid solutions of the $\text{Nd}_{1-x}\text{Ca}_{1+x}\text{FeO}_{4-y}$ system for compositions with $x = 0.00, 0.25, 0.50, 0.75,$ and 1.00 were tried in the first preparation. The structural

TABLE I Lattice parameters, lattice volume, c/a ratio, and crystal system for the $\text{Nd}_{1-x}\text{Ca}_{1+x}\text{FeO}_{4-y}$ system

x	Lattice parameters (nm)		c/a	Lattice volume (nm^3)	Crystal system
	a	c			
0.000	0.3868	1.2092	3.126	0.18090	tetragonal
0.125	0.3853	1.2105	3.142	0.17971	tetragonal
0.250	0.3842	1.2082	3.145	0.17830	tetragonal
0.375	0.3847	1.2110	3.148	0.17924	tetragonal
0.500	0.3856	1.2087	3.134	0.17975	tetragonal

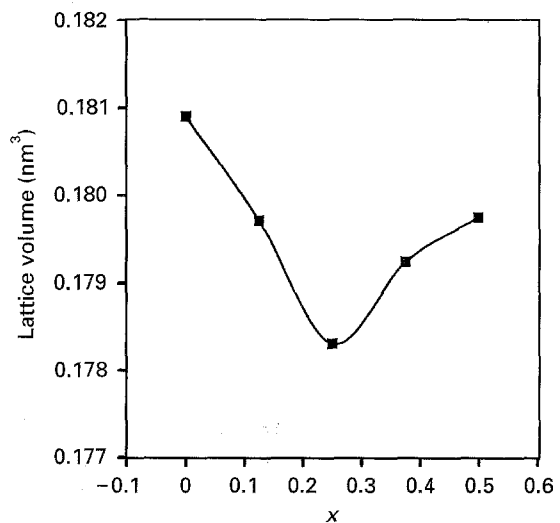


Figure 1 Plot of the lattice volume versus x for the $\text{Nd}_{1-x}\text{Ca}_{1+x}\text{FeO}_{4-y}$ system.

distortion occurs when $x \geq 0.500$ and their patterns are distinctly different from that of tetragonal $I_{4/mmm}$. It is apparent that the mixed phases are formed in the range of $0.5 < x < 1.0$. Therefore, our experiments are restricted to the region $0.000 \leq x \leq 0.500$ and the five solid solutions $x = 0.000, 0.125, 0.250, 0.375,$ and 0.500 were prepared. Lattice parameters, lattice volume, c/a ratio, and crystal system are listed in Table I. X-ray diffraction patterns of all the compositions show a characteristic tetragonal $I_{4/mmm}$ structure. A plot of the lattice volume versus x value of the system is shown in Fig. 1.

The Mohr salt analysis of the solid solutions was carried out and then τ and y values of the $\text{Nd}_{1-x}\text{Ca}_{1+x}\text{Fe}_{1-\tau}^{3+}\text{Fe}_{\tau}^{4+}\text{O}_{4-y}$ system were calculated. The τ and y values and the nonstoichiometric chemical formulas are listed in Table II. Plots of τ and y values versus x value are shown in Fig. 2. The composition with $x = 0.375$ has a maximum τ value because many oxygen vacancies are formed at $x = 0.500$.

Just as for perovskite oxide, a tolerance factor for K_2NiF_4 -type compounds can be defined as follows:

$$t = \frac{r(\text{A} - \text{O})}{[2r(\text{B} - \text{O})]^{1/2}}$$

Also, Poix has defined the tolerance factor as:

$$t = \frac{\psi}{(2\beta_{\text{B}})^{1/2}}$$

TABLE II x , τ , y values, and nonstoichiometric chemical formula for the $\text{Nd}_{1-x}\text{Ca}_{1+x}\text{FeO}_{4-y}$ system

x	τ	y	Nonstoichiometric chemical formula
0.000	0.000	0.000	$\text{NdCaFe}^{3+}\text{O}_{4.000}$
0.125	0.116	0.004	$\text{Nd}_{0.875}\text{Ca}_{1.125}\text{Fe}_{0.884}^{3+}\text{Fe}_{0.116}^{4+}\text{O}_{3.996}$
0.250	0.177	0.036	$\text{Nd}_{0.750}\text{Ca}_{1.250}\text{Fe}_{0.823}^{3+}\text{Fe}_{0.177}^{4+}\text{O}_{3.964}$
0.375	0.206	0.085	$\text{Nd}_{0.625}\text{Ca}_{1.375}\text{Fe}_{0.794}^{3+}\text{Fe}_{0.206}^{4+}\text{O}_{3.915}$
0.500	0.099	0.200	$\text{Nd}_{0.500}\text{Ca}_{1.500}\text{Fe}_{0.901}^{3+}\text{Fe}_{0.099}^{4+}\text{O}_{3.800}$

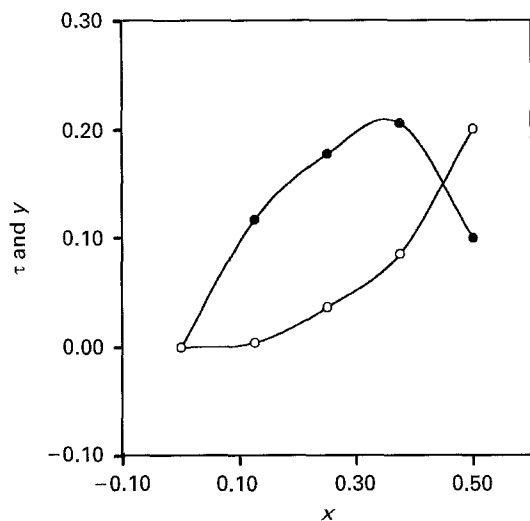


Figure 2 Plots of τ (●) and y (○) versus x for the $\text{Nd}_{1-x}\text{Ca}_{1+x}\text{FeO}_{4-y}$ system.

where ψ_A and β_B are invariant values associated with A–O and B–O distance in nine-fold and six-fold coordinations, respectively. The tetragonal K_2NiF_4 structures are stable for $0.85 < t < 1.02$ [6]. The c/a ratio or tetragonality of the K_2NiF_4 structure is also used as the reference for the stability of the tetragonal structure. It is stable in the range $3.25 < c/a < 3.30$. If Nd^{3+} ions ($r = 130.3$ pm) are substituted by larger Ca^{2+} ions ($r = 132.0$ pm), A–O bond length increases and B–O bond length decreases with the formation of Fe^{4+} ion. The tolerance factor for NdCaFeO_4 compound is about 0.89. It is near the low limit and the t value also increases as the x value increases, which favours the more stable tetragonal phase. The c/a ratio as a function of x is plotted in Fig. 3.

The study will concentrate on where oxygen vacancies are formed and how they are arranged. Three factors that affect the lattice parameters of the tetragonal K_2NiF_4 structure are (i) the substitution of a Nd^{3+} ion by a slightly larger Ca^{2+} ion which increases both the a and c parameters, (ii) the formation of a Fe^{4+} ion which mainly affects the a parameter, and (iii) the formation of oxygen vacancies which decreases the a and c parameters. In the compositions with $x = 0.125$ and 0.250 , relatively low oxygen vacancies are formed. However the a parameter decreases with the formation of small Fe^{4+} ions despite the substitution effect of Ca^{2+} ions in place of Nd^{3+} ions. The solid solutions with considerable amounts of Fe^{4+} ions show an increase of the a parameter in the compositions with $x = 0.375$ and 0.500 . The substitution of Ca^{2+} ions in place of Nd^{3+} ions increases the

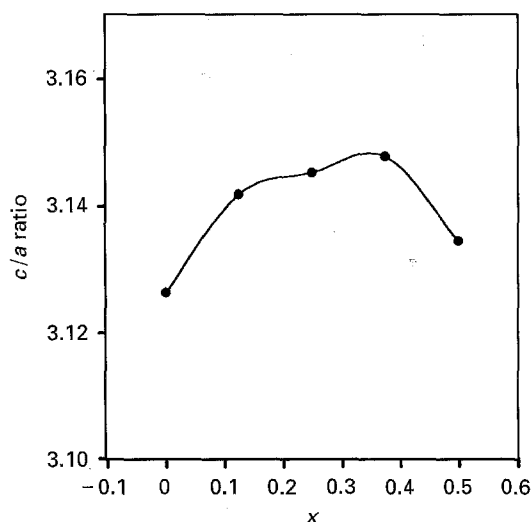


Figure 3 Plot of c/a ratio versus x for the $\text{Nd}_{1-x}\text{Ca}_{1+x}\text{FeO}_{4-y}$ system.

c parameter when $x = 0.125$. However it decreases again when $x = 0.250$. The decrease with the formation of oxygen vacancies in the rock salt layer overcomes the substitution effect of Ca^{2+} ions in place of Nd^{3+} ions. Although oxygen vacancies increase again when $x = 0.375$ and they are arranged in both rock salt and perovskite layers, the substitution effect dominates and thus increases the c parameter. The large formation of oxygen vacancies mainly at the rock salt layer decreases the c parameter when $x = 0.500$.

The Mössbauer spectra at room temperature for all compositions are shown in Fig. 4. The Mössbauer parameters such as isomer shift, quadrupole splitting, and magnetic hyperfine field are listed in Table III. Mössbauer spectra are fitted to the Lorentzian curve using PC-MOS. The Mössbauer spectrum of a distinct sextet line at room temperature for the composition with $x = 0.000$ is characteristic of the iron ion in a magnetically ordered state or below magnetic ordering temperature (T_N). There must be a single valence state Fe^{3+} iron from only one set of sextet peaks and isomer shift of 0.3060 mm s^{-1} . A distorted octahedra where apical oxygens are compressed along the c -axis can be predicted in terms of a negative sign of the quadrupole splitting. The Mössbauer spectrum for $x = 0.125$ shows doublet peaks and it is interpreted as a superposition between Fe^{3+} and Fe^{4+} doublets. Mohr salt analysis shows very small amounts of oxygen vacancies present for $x = 0.125$. However, large oxygen vacancies occur over $x \geq 0.250$ and their random distribution produces oxygen deficient octahedra (ODO).

The Mössbauer spectra are fitted under the assumption of superposition between two Fe^{3+} ions with different environments and a Fe^{4+} ion. Two major factors that affect the isomer shift of the Fe ion are (i) the Fe–O bond length where the shorter the bond length, the stronger the covalency is and the isomer shift moves to a negative value and (ii) competitive oxygen bonding between Fe^{3+} and Fe^{4+} ions. The isomer shift of Fe^{3+} ion moves to a positive value due to the relatively weak Fe^{3+} strength for oxygen bonding and that of the Fe^{4+} ion moves to a negative value

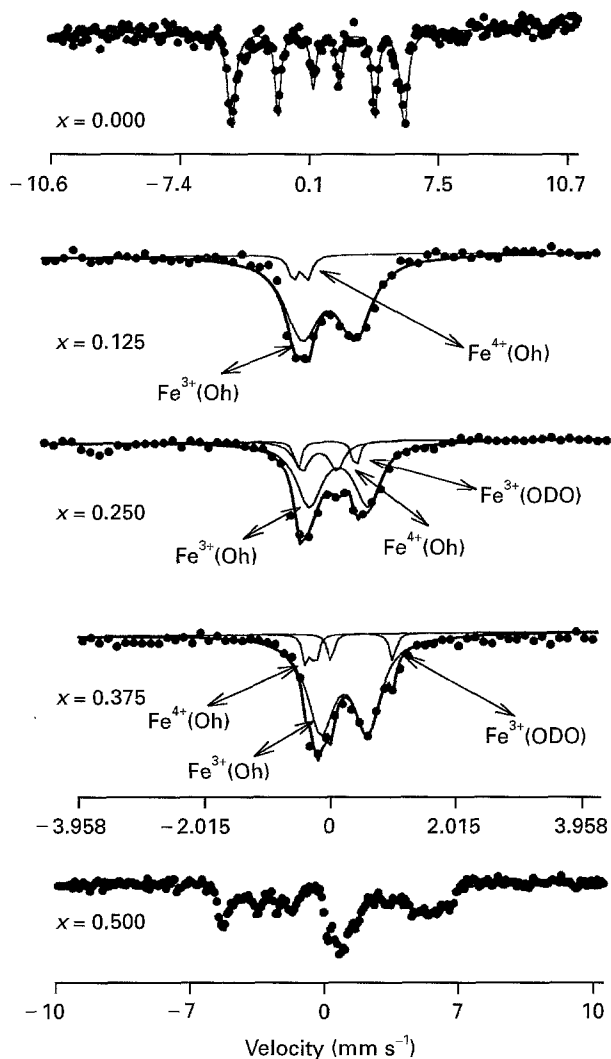


Figure 4 The Mössbauer spectra of the $\text{Nd}_{1-x}\text{Ca}_{1+x}\text{FeO}_{4-y}$ system.

in the $\text{Fe}^{3+}-\text{O}^{2-}-\text{Fe}^{4+}$ interaction. Isomer shifts of Fe^{3+} ions when $x = 0.000, 0.125$ and 0.250 move to negative values by the combination of the above two effects as the a parameter decreases. The amount of variation in the isomer shifts becomes smaller stepwise as the amounts of Fe^{4+} ion or τ value increases and the isomer shifts of Fe^{3+} ions when $x \geq 0.25$ show the reverse. The negative and large quadrupole splitting shows that the c -axis $\text{Fe}-\text{O}$ bond length is shorter than the ab -plane $\text{Fe}-\text{O}$ bond length.

The Mössbauer spectrum for $x = 0.000$ shows that the Fe^{3+} octahedra are compressed and largely distorted. The sign change of quadrupole splitting between $x = 0.000$ and $x = 0.125$ shows that large distortion of the octahedra occurs. This is consistent with the large change in tetragonality or c/a ratio between $x = 0.000$ and $x = 0.125$. The quadrupole splittings for other compositions are all positive values which decrease as x increases. There is a small shoulder in the large doublet peaks in the spectrum for $x = 0.375$ and a peak is introduced representing small amounts of oxygen deficient octahedra. The isomer shift order of $\text{Fe}^{3+}(\text{Oh}) > \text{Fe}^{3+}(\text{ODO}) > \text{Fe}^{4+}(\text{Oh})$ is consistent with order of the electron density at the nucleus.

TABLE III Mössbauer parameters for the $\text{Nd}_{1-x}\text{Ca}_{1+x}\text{FeO}_{4-y}$ system

x	State of Fe ion	δ (mm s^{-1}) ^a	ΔE_q (mm s^{-1}) ^b	H_{int} (T) ^c
0.000	$\text{Fe}^{3+}(\text{Oh})$	0.3060	-0.5160	32.95
0.125	$\text{Fe}^{3+}(\text{Oh})$	0.2615	0.7875	-
	$\text{Fe}^{4+}(\text{Oh})$	-0.1081	0.2081	-
0.250	$\text{Fe}^{3+}(\text{Oh})$	0.2455	0.7708	-
	$\text{Fe}^{3+}(\text{ODO})$	0.2271	0.1309	-
	$\text{Fe}^{4+}(\text{Oh})$	-0.2944	0.1521	-
0.375	$\text{Fe}^{3+}(\text{Oh})$	0.2375	0.7074	-
	$\text{Fe}^{3+}(\text{ODO})$	0.2282	0.3718	-
	$\text{Fe}^{3+}(\text{Oh})$	-0.2967	0.1585	-

^a Isomer shift.

^b Quadrupole splitting.

^c Magnetic hyperfine field.

Magnetic measurements are carried out from room temperature to 800 K under a magnetic field of 10 T and plots of the χ^{-1} versus temperature (K) are shown in Fig. 5. Magnetic parameters and effective magnetic moments are listed in Table IV. The magnetic transition temperatures for $x = 0.000$ and 0.500 must be over room temperature and near room temperature, respectively, from the Mössbauer spectra [8]. The inverse molar susceptibility for $x = 0.000$ shows a weak ferromagnetic behaviour below 680 K in good agreement with the Mössbauer spectrum for $x = 0.000$. The perovskite NdFeO_3 compound corresponding to NdCaFeO_4 also shows a weak ferromagnetic behaviour below 707 K [9]. The magnetic behaviour can be explained by the structural distortion of FeO_6 octahedra. The antiferromagnetic interaction of Fe^{3+} (high spin) $-\text{O}^{2-}-\text{Fe}^{3+}$ (high spin) is formed in the FeO_6 octahedra and thus shows a weak ferromagnetic behaviour by the spin canting of Fe ions. The negative θ_p value in the Table IV confirms the antiferromagnetic interaction.

The magnetic transition temperature of the NdCaFeO_4 compound is much higher than those of the CaLaFeO_4 (373 K) and LaSrFeO_4 (380 K) compounds. In the CaLaFeO_4 [3] magnetic structure, the interplanar coupling between neighbouring Fe(III) ions is also ferromagnetic and the magnetic moments in the (001) plane are aligned along the a -axis. The moment is equal to $3.75 \mu_B$ at 4.2 K [3] and the magnetic ordering appears at 373 K. The absolute value of inverse molar susceptibility decreases as x increases.

The magnetic interaction of the super-exchange model is principally produced by the $\text{Fe}-\text{O}-\text{Fe}$ interaction of ab -plane FeO_2 in the K_2NiF_4 -type compounds. Three factors affecting the degree of magnetic interaction are the $\text{Fe}-\text{O}$ bond length, the tetragonality, and oxygen vacancy. The abrupt decreasing of the Néel temperature for $x = 0.125$ shows that the rapid increase of c/a or the decrease of the FeO_6 octahedra distortion gives the largest effect for the magnetic interaction. The formation of Fe^{4+} ions with increasing x value reduces the antiferromagnetic

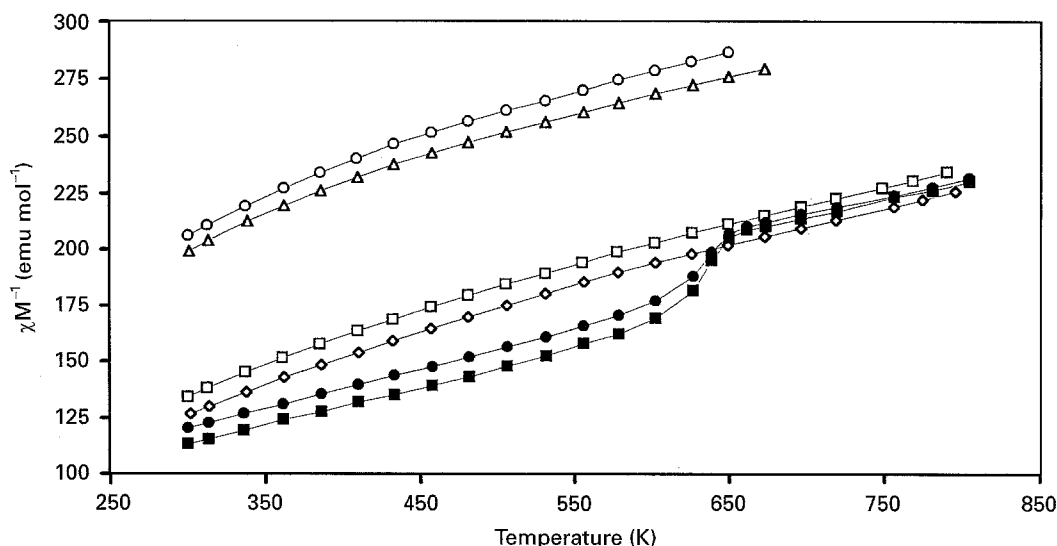


Figure 5 Inverse molar susceptibility as a function of temperature for the $\text{Nd}_{1-x}\text{Ca}_x\text{FeO}_{4-y}$ system. Key: \circ —0.500; \triangle —0.375; \square —0.250; \diamond —0.125; \bullet —0.000 (10 T); \blacksquare —0.000 (7 T).

TABLE IV Magnetic parameters and effective magnetic moments for the $\text{Nd}_{1-x}\text{Ca}_x\text{FeO}_{4-y}$ system

x	C	θ_P	$\mu_{\text{eff}}(\text{Tot})$	$\mu_{\text{cal}}(\text{Fe})$
0.000	6.51	−16.25	7.220	6.095
0.125	5.04	−13.88	6.349	5.215
0.250	5.03	−16.00	6.342	5.384
0.375	4.78	−29.89	6.187	5.308
0.500	4.46	−32.53	5.972	5.308

TABLE V Activation energy of the electrical conductivity for the $\text{Nd}_{1-x}\text{Ca}_x\text{FeO}_{4-y}$ system

x	Temperature region	Activation energy (eV)
0.000	$278 \leq T \leq 530$	0.165
	$530 \leq T \leq 900$	0.304
0.125	$152 \leq T \leq 190$	0.301
	$190 \leq T \leq 293$	0.136
0.250	$143 \leq T \leq 223$	0.313
	$223 \leq T \leq 273$	0.124
0.375	$146 \leq T \leq 214$	0.327
	$214 \leq T \leq 286$	0.205
0.500	$143 \leq T \leq 223$	0.371
	$223 \leq T \leq 273$	0.210

$\text{Fe}^{3+}\text{—O—Fe}^{3+}$ interaction. The magnetic transition temperature for $x = 0.500$ is near room temperature where both the τ value and the c/a ratio are smaller than those for $x = 0.125, 0.250$ and 0.375 .

Plots of χ^{-1} versus temperature for $x = 0.125\text{--}0.500$ follow the Curie–Weiss law with small positive curvature. However, since the linearity is in the error range $R^2 \geq 0.998$, the μ_{eff} of Fe^{3+} ions calculated from the C value is $6.02 \mu_B$ for $x = 0.00$. The Fe^{3+} ion should be in a high spin state considering the theoretical value $5.92 \mu_B$ of high spin Fe^{3+} ion. The length of the ab -plane Fe—O bond in terms of the a parameter decreases as x increases. Therefore, the Fe ions for $x = 0.125\text{--}0.500$ have a low spin state or an intermediate spin state. The Curie–Weiss constant is the refer-

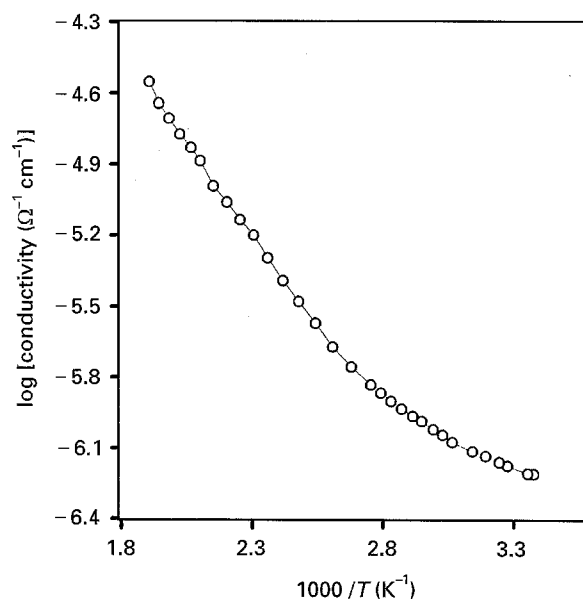


Figure 6 Plot of log electrical conductivity versus $1000/T$ for the $\text{NdCaFeO}_{4.000}$ system.

ence for the degree of antiferromagnetic interaction and it shows relatively small values in these experiments. The strength of this interaction is determined by the ab -plane Fe—O bond length, the bond angle of Fe—O—Fe , and the amounts of Fe^{3+} ions. The Curie–Weiss constants for $x = 0.125$ and 0.250 are small because of the decrease in the Fe—O bond length despite the formation of Fe^{4+} ions and oxygen vacancies. The decrease of the c/a ratio for $x = 0.375$ and 0.500 takes the Fe—O—Fe bond angle close to 180° , corresponding to large Curie–Weiss constants.

The electrical conductivities are measured for $x = 0.000$ in the range 278 to 800 K and for $x = 0.125\text{--}0.500$ in the range 140 to 273 K. Plots of log conductivity versus $1000/T$ are shown in Figs 6 and 7. The slope change of the plot can be explained by a phase transition in the composition where $x = 0.000$ with low tolerance factor [10]. The plots for $x = 0.125, 0.250, 0.375$, and 0.500 also show slope changes.

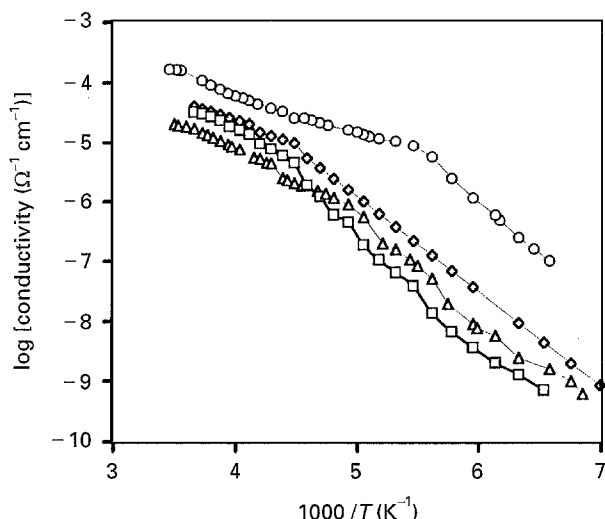


Figure 7 Plots of log electrical conductivity versus $1000/T$ for the compositions with $x = 0.125, 0.250, 0.375,$ and 0.500 in the $\text{Nd}_{1-x}\text{Ca}_{1+x}\text{FeO}_{4-y}$ system. Key: \circ $x = 0.125$; \diamond $x = 0.250$; \square $x = 0.500$; \triangle $x = 0.375$.

The activation energy of the conductivity is composed of the energy for the $\text{Fe}^{3+} \rightarrow \text{Fe}^{4+} + e^-$ and hopping energy of an electron from one site to another. The increase of the τ value decreases activation energy in the $\text{Nd}_{1-x}\text{Ca}_{1+x}\text{FeO}_{4-y}$ system. However, oxygen vacancies act as electron trapping sites and also increase the activation energy. The conduction mechanism may be the hopping model of the conduction electrons based on the mixed valences between Fe^{3+} and Fe^{4+} ions.

4. Conclusions

The structure for all the solid solutions of the $\text{Nd}_{1-x}\text{Ca}_{1+x}\text{FeO}_{4-y}$ system is tetragonal $I_{4/mmm}$. Generally, the mole ratio of the Fe^{4+} and the oxygen vacancies increase as x increases. The mixed valence between the Fe^{3+} and Fe^{4+} ions can be measured and identified by Mohr salt analysis and Mössbauer spectroscopy, respectively. Nonstoichiometric chemical

formulas for the system are formulated from the $x, y,$ and τ values.

Magnetic measurement shows that the magnetic interaction occurs through the super-exchange interaction and the structural distortion in the $\text{Nd}_{1-x}\text{Ca}_{1+x}\text{FeO}_{4-y}$ system presents weak ferromagnetic and paramagnetic behaviours for $x = 0.000$ and $x = 0.125$, respectively. The τ value increase in the mixed valences between Fe^{3+} and Fe^{4+} ions decreases the activation energy of the electrical conductivity and therefore, the conduction mechanism should be the hopping model of the conduction electron. The oxygen vacancies at the FeO_2 plane in the perovskite layer act as electron trapping centres and increase the activation energy of the electrical conductivity.

Acknowledgements

This research was supported by grant No. 92-25-00-02 from the Korea Science and Engineering Foundation in 1993 and therefore we express our appreciation to the authorities concerned.

References

1. M. PARRAS, M. VALLET-REGI and J. M. GOZALIEZ-CALBERT, *Mater. Res. Bull.* **22** (1987) 1413.
2. P. GANGULY and C. N. R. RAO, *J. Solid State Chem.* **53** (1984) 193.
3. N. T. DINH, M. VLASSE, M. PERRIN and G. LEFLEM, *ibid.* **31** (1980) 1.
4. J. L. SOUBEYROUX, P. COURBIN, D. FRUCHART and G. LEFLEM, *ibid.* **31** (1980) 313.
5. DIBYENDU GANGULI, *ibid.* **30** (1979) 353.
6. P. POIX, *ibid.* **31** (1980) 95.
7. K. R. POEPELMEIER, M. E. LEONOWICZ and J. M. LONGO, *ibid.* **44** (1982) 89.
8. T. C. GIBB, *J. Mater. Chem.* **2** (1992) 415.
9. CHUL HYUN YO, ILE YOUNG JUNG, KWANG HYUN RYU, KWANG SUN RYU and JIN HO CHOY, *J. Solid State Chem.* **114** (1995) 265.
10. E. PICKETT, *Rev. Mod. Phys.* **61** (1989) 433.

Received 6 March
and accepted 1 December 1995